CHARACTERIZATION OF THE DEUTERON BEAM CURRENT IN A LINEAR ACCELERATOR FOR NUCLEAR-DIAGNOSTIC CALIBRATIONS

By

Daniel Denis

SUBMITTED TO THE DEPARTMENT OF NUCLEAR SCIENCE AND ENGINEERING IN PARTIAL FULFILLMENT OF THE REQUIREMENTS FOR THE DEGREE OF BACHELOR OF SCIENCE IN NUCLEAR SCIENCE AND ENGINEERING AT THE MASSACHUSETTS INSTITUTE OF TECHNOLOGY

[FEBRUARY 2009]
December 2008

Signature of Author: _____
Daniel Bradley Denis
Department of Nuclear Science and Engineering
December 30th, 2008

Certified By _____
Richard Petrasso
Division Head and Senior Research Scientist, Plasma Science and Fusion Center
Thesis Supervisor

Certified By: _____
Kim Molvig
Associate Professor of Nuclear Engineering
Thesis Reader

Accepted By: _____
Kim Molvig
Acting Chairman, NSE Committee for Undergraduate Studies

CHARACTERIZATION OF THE DEUTERON BEAM CURRENT IN A LINEAR ACCELERATOR FOR NUCLEAR-DIAGNOSTIC CALIBRATIONS

By

Daniel Denis

Submitted to the Department of Nuclear Science and Engineering on December 30th, 2008 in Partial Fulfillment of the Requirements for the Degree of Bachelor of Science in Nuclear Science and Engineering

ABSTRACT

In Inertial Confinement Fusion (ICF) research, passive detection systems are often required in several applications for observing fusion-product spectra from an ICF-capsule implosion. These detection devices can be calibrated by using fusion products produced in a linear accelerator as the characteristics of the fusion products are well known. For these calibration experiments it is important to determine the absolute current of the beam striking the target, because this determines the fusion-reaction rate. A Faraday Cup was installed and used for this purpose, in which an ammeter is used to measure the charge built up on the cup that is proportional to the beam current of the accelerator. Currents up to ~100μA were measured using the Faraday Cup. For 100μA 120kV D^+ current on an erbium target doped with deuterium, D-D reaction rates of ~107 per second were determined. Besides the Faraday Cup, a target movement stepper motor was also successfully installed and tested, their LabView based control programs were written, and their operation procedures were documented. The secondary electron suppression capability of the cup was successfully tested as well. The Faraday Cup serves as a diagnostic for the quality of accelerator operation.

Thesis Supervisor: Richard Petrasso
Title: Division Head and Senior Research Scientist, Plasma Science and Fusion

ACKNOWLEDGEMENTS

I want to thank Dr. Rich Petrasso, Nareg Sinenian, and Dr. Kim Molvig for their roles as Thesis Advisor, Thesis Mentor, and Thesis Reader, respectively. I am grateful for their time spent contributing to the project, reading the thesis, and for the fact that they made the entire process very pleasant for me. I also want to thank Rich for giving me both my first (in freshman year) and last (for the thesis) research experiences as an MIT undergraduate.

Many thanks to Johan Frenje for his help in reading and revising the thesis, Fredrick Séguin and Chikang Li for thesis support, Dan Casey and Mario Manuel for discussing ICF concepts and formulas, and Hans Rinderknecht and Mike Rosenberg for their assistance in accelerator operation and data collection. I also appreciate the support of Jocelyn Schaeffer and Irina Cashen, who helped me with lab logistics, organization, and troubleshooting.

I would also like to acknowledge the support of my family members, who have always encouraged me in my endeavors. In addition, my friends were always patient with my goals and deadlines, and helped to distract me at necessary times. Finally, I want to thank the Department of Nuclear Science and Engineering, for providing a vigorous curriculum and imparting a breadth of nuclear knowledge.

Table of Contents

List of Figures and Tables

1. Introduction

1.1 High Energy Density Physics (HEDP) Division

The HEDP Division at the MIT Plasma Science and Fusion Center (PSFC) focuses on the studies of Inertial Confinement Fusion (ICF). In ICF, a capsule, filled with varying amounts of deuterium (D) and tritium (T), is illuminated by symmetrically arranged lasers that cause the capsule to compress. When the capsule has been compressed about 10-20 times in radius, the density and temperature are high enough for thermonuclear fusions to occur. The fusion reactions commonly produced in ICF are:

$$D + T \rightarrow n\ (14.1\ MeV) + \alpha\ (3.5\ MeV) \quad (1)$$

$$D + D \rightarrow n\ (2.5\ MeV) + {}^{3}He\ (0.8\ MeV) \quad (2)$$

$$D + D \rightarrow p\ (3.0\ MeV) + T\ (1.0\ MeV) \quad (3)$$

Cryogenic DT or D_2 capsules are now routinely imploded with the OMEGA laser system (LLE Website, "OMEGA Laser Facility") at the Laboratory for Laser Energetics, University of Rochester. These implosions are hydrodynamically equivalent to the baseline direct-drive ignition design for the National Ignition Facility (NIF) (NIF Website), at the Lawrence Livermore National Laboratory at UC Berkeley, to allow for experimental validation of the design prior to the first ignition experiments at the NIF. The design consists of a cryogenic-DT-fuel layer inside a thin spherical carbon-hydrogen ablator, which is compressed quasi-isentropically to minimize the laser energy required to achieve ignition conditions. If the capsule is sufficiently compressed, the high areal density (ρR) of the cryogenic DT fuel can support a propagating thermonuclear burn wave due to local bootstrap heating by the DT-alpha particles produced in reaction 1.

As these "cryo" shots involve some unique engineering challenges in manufacturing, thermal melting, and shot symmetry, hydrodynamically equivalent "surrogate" capsule implosions are often used to study the physics involved in cryogenic implosions.

At the OMEGA facility, 60 lasers with a total energy capacity of 30 kJ can illuminate a capsule less than 1 mm in diameter (LLE Website). Although the energy involved is less than required for ignition experiments at the NIF (see Figure 1- 1), cutting-edge science in both HEDP and ICF is being performed at the facility. Extensive research and development of new types of diagnostics for future generation ICF facilities are conducted as well at OMEGA.

The NIF is the next generation ICF facility, and the plan is to start conducting the first ignition experiments in 2010. This facility will employ 192 lasers delivering a maximum energy of 1.8 MJ in a few nanoseconds. The HEDP Division is currently designing and testing a diagnostic (Frenje 1) for the

ignition campaign at NIF. In addition, the Division has mainly implemented diagnostics at OMEGA based on passive detection devices (MIT PSFC Website), because electronic instruments are susceptible to electromagnetic pulses (EMP), x-rays, and neutron-activated gamma rays. This is especially a significant problem when running certain high intensity lasers (such as the OMEGA EP peta-watt laser), during which large EMP will certainly disrupt the functionality of many types of electronic-based diagnostics.

1.2 Inertial Confinement Fusion (ICF)

Key parameters that characterize the performance of an implosion are: neutron yield (Y_n), the areal density (ρR), and the ion temperature (T_i). The first parameter, i.e., neutron yield, depends on the latter two, where (ρR) indicates the amount of material compression that has occurred (Frenje 1-2).

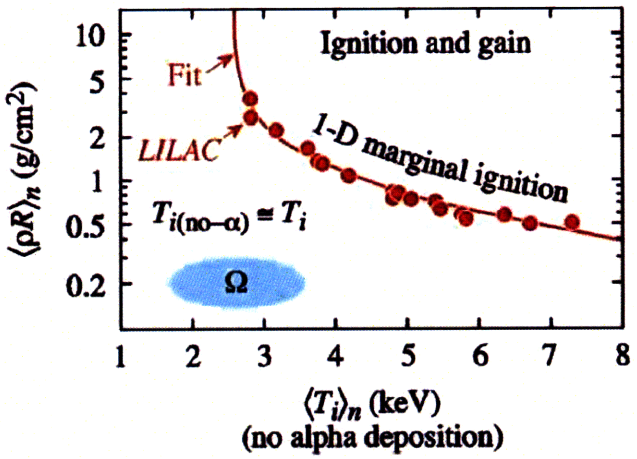

Figure 1- 1: ***ICF-ignition Criterion.*** *The graph displays neutron averaged* ρR *as a function of ion temperature. The red line shows the 1-D marginal ignition and the "Ω" symbol shows the region in which the OMEGA facility operates (McRory 2). Above the red line, the parameters are such that ignition and energy gain is achieved.*

As briefly discussed in the previous section, achieving ignition requires high ρR and ion temperature. This is illustrated in Figure 1- 1, which shows the 1-D marginal ignition criterion that indicates that a T_i of ~4-5 keV and a ρR of ~1 g/cm^2 are required for ignition, i.e., self-sustained burn.

In an ICF implosion, primary neutrons are produced primarily via reaction 1. These primary DT neutrons carry a wealth of information about the ICF implosion, such as information about T_i. For a single-temperature plasma, T_i can be determined from the Doppler width (ΔE_p) of the primary neutron spectrum [to the first order $T_i \approx (\Delta E_p/177)^2$ keV], which is represented accurately by a single-Gaussian distribution.

In a secondary process, a small fraction of the primary neutrons elastically scatter off the fuel ions [primarily deuterons (D) and tritons (T)] as described by:

$$n' + D \rightarrow n' (1.6\text{-}14.1 \text{ MeV}) + D' (<12.5 \text{ MeV}) \quad (4)$$

$$n' + D \rightarrow n' (3.5\text{-}14.1 \text{ MeV}) + T' (<10.6 \text{ MeV}) \quad (5)$$

By using a relatively simple model of an implosion, the ρR can be related to the down-scattered neutron yield ($Y_{n'}$) by:

$$\rho R \approx \frac{(2\gamma + 3)m_p}{(\gamma\sigma_d + \sigma_t)} \frac{Y_{n'}}{Y_n} \quad (6)$$

Where $\gamma = n_d/n_t$; σ_d and σ_t are the effective elastic scattering cross sections for deuterons and tritons, respectively; m_p is the proton mass; $Y_{n'}$ is the measured down-scattered neutron yield in a certain defined energy range; and Y_n is the measured primary neutron yield. As shown by Equation 6, the fuel ρR is linearly proportional to the yield ratio of down-scattered neutrons (n') and primary neutrons (n).

As scattered high-energy deuterons (D') or tritons (T'), produced in reactions 4 and 5, pass through the fuel, some undergo tertiary reactions and produce tertiary neutrons (n"):

$$D' + T \rightarrow \alpha + n'' (12.0 - 30.1 \text{ MeV}) \quad (7)$$

$$T' + D \rightarrow \alpha + n'' (9.2 - 28.2 \text{ MeV}) \quad (8)$$

According to simulations, the yield of the tertiary neutrons (>20 MeV) is of the order 10^{-6} relative to the primary neutron yield and is proportional to ρR and ρR^2 for high- ρR and low- ρR implosions, respectively.

When the alpha particles, produced in reaction 1, interact with the plasma they lose energy mainly through small angle scattering with electrons. However, there is a finite probability that the alpha particles transfer several MeV to the deuterons or tritons by large angle Coulomb or nuclear-elastic scattering. These collisions give rise to non-thermal distributions of fuel ions, which can in turn react with the thermal ions generating a secondary component in the neutron spectrum. Although with much lower intensity than the primary component (~10^{-5} to ~10^{-2} depending on the implosion), the secondary-neutron component dominates at energies in the range 16-20 MeV. As the intensity of the secondary-neutron component is strongly sensitive to electron temperature (T_e), measurement of this component could, in principle, address T_e in the high-density region, the effect of alpha-particle heating and fuel-ablator mix.

Figure 1- 2 shows a few neutron spectra simulated for OMEGA and the NIF. These spectra are based on all possible reaction processes starting with the DT and DD reactions.

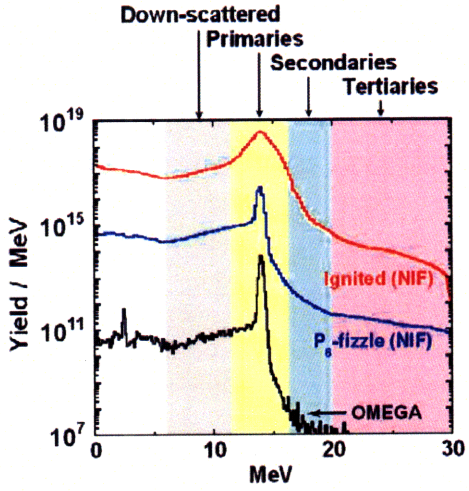

Figure 1- 2: ***Simulated ICF Neutron Spectrum from OMEGA and NIF.*** *Typical neutron spectra simulated by LASNEX for an OMEGA (black line) and two NIF (blue and red lines) cryogenic DT implosions. For OMEGA, a primary neutron yield of 2.4 x 10^{13} and down-scattered neutron yield of 1.5 x 10^{11} (grey area) corresponding to a fuel* ρR *of 128 mg/cm^2 were simulated. For NIF, a neutron spectrum was simulated for an ignited (red line) and a P_6-fizzle (blue line) implosion. For the ignition case, a primary yield of 7.4 x 10^{18} and down-scattered yield of 3.6 x 10^{17} were simulated. A significant tertiary component (pink area) of 1.5 x 10^{15} was simulated as well. For the "P_6 fizzle", a primary yield of 2.1 x 10^{16}, down-scattered yield of 1.5 x 10^{15} and tertiary yield of 2.0 x 10^{12} were simulated. A ρR of ~2 g/cm^2 was simulated in both cases. The non-thermal secondary-neutron component, originating from the alpha-particle interaction with the fuel ions, dominates at energies in the range 16-20 MeV (blue area). A secondary-neutron yield of 1.5 x 10^{8}, 6.8 x 10^{12}, and 9.0 x 10^{16} was simulated for the OMEGA, NIF-P_6-fizzle and the NIF-ignition implosion, respectively (Casey 4; Frenje 3).*

1.3 Techniques for Measuring ICF-fusion Products

The charged-particle spectrometry techniques used by the HEDP Division rely primarily on a passive-detection device called CR-39. This material is used as a nuclear track detector in conjunction with magnets or range filters, depending on application. When interacting with the CR-39, the charged particles make tracks that are revealed by etching the material in sodium hydroxide. The material is subsequently scanned under a microscope, and from the position and/or diameter of a track, energy and particle type can be determined (Seguin 1).

2. Particle Accelerator

2.1 Accelerator Overview

A Cockraft-Walton (CW) linear particle accelerator has been refurbished for primarily testing these CR-39 detectors. The system was originally manufactured by Texas Nuclear Corporation as a neutron generator, but it was converted for use as a fusion-product source (McDuffee 1). Since then, the device has been modified continuously to improve the quality of the source and to increase its capability and flexibility as a diagnostic development tool. The current configuration is schematically shown in Figure 2- 1. The accelerator's beam particle composition and energies can be adjusted, so various scenarios can be tested. Figure 2- 1 shows the accelerator schematic after completed upgrades.

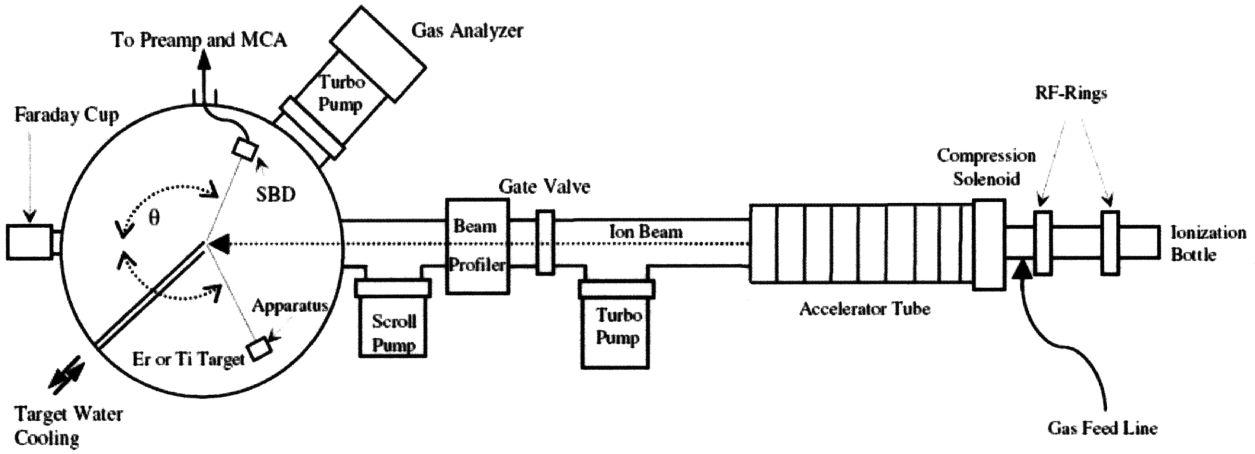

*Figure 2- 1: **A Schematic Drawing of the Accelerator.** Gas is fed into the ion source bottle, where the gas is ionized by two radiofrequency (RF) rings. Positively charged ions are subsequently extracted into the accelerator column where they are accelerated before they hit the target in which fusion reactions occur. The fusion products are detected by a set of detectors positioned around the target. A Faraday Cup has been installed on the backside of the target chamber for absolute current measurements (McDuffee 2).*

The old accelerator control system was replaced by a new system based on LabView virtualization software, which allows a National Instruments PXI Card computer to control the operation of the accelerator. The original target chamber was replaced with a much larger, more flexible chamber with ports allowing for a larger set of diagnostics to be fielded on the chamber.

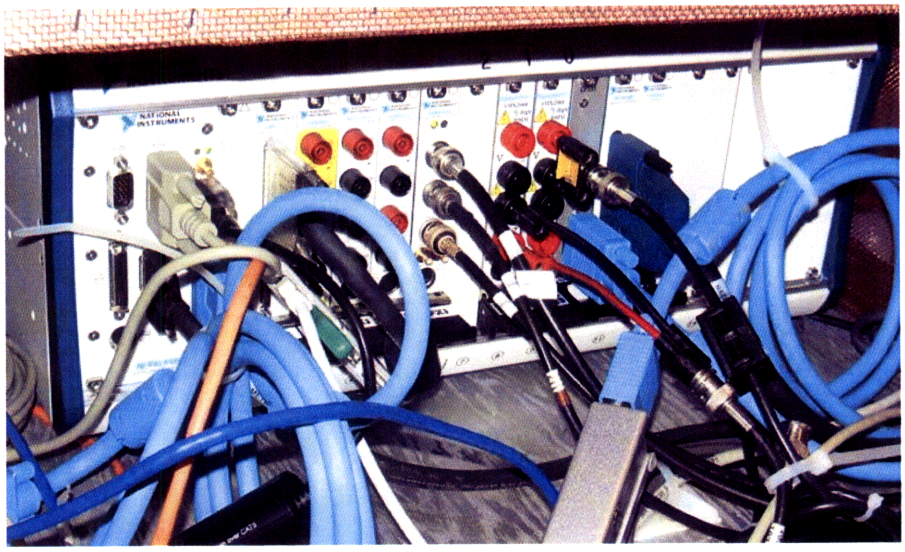

Figure 2- 2: ***NI PXI Card Computer.*** *The PXI cards can be easily interchanged to add or remove functionality. The computer's virtualization software operates the accelerator and receives measurements from diagnostic devices. The blue serial port on the right connects to an NI device that controls the solenoid, water cooling pump, and RF rings. The three center digital mulitmeters detect the counts from the SBD, the current from the Faraday Cup, and the voltage from the high voltage detector for the accelerating voltage, from left to right respectively. The left metallic serial port connects to the NI power drive that controls the focus, extraction, and target insertion stepper motors.*

The NI PXI Card computer has multiple card slots in which device cards can be easily inserted and removed in order to add new capabilities to the computer. For example, the PXI card computer used by the HEDP Division has extra cards for Digital Multimeters (DMMs), an extra network card, and an extra VGA port video card. This computer controls the operation of the accelerator's solenoid, water cooling pump, RF rings, and applied accelerator beam voltage, as well as the movement of stepper motors connected to an NI power drive.

The ion source is mainly operated with deuterium (D_2) or Helium-3 (^3He) gas. D-D and D-^3He reactions produce 3 MeV and 14.7 MeV protons, respectively, which can then be used to calibrate CR-39 samples. Most of the accelerator tests use D_2 gas because ^3He gas is prohibitively expensive ($\$10^3$ for a small tube). The ion source is biased over two radiofrequency (RF) coils, which ionize the injected neutral gas into a plasma that is extracted into the accelerator column. Additionally, there is an "extraction" electrode, which is positively biased (0-5kV) with respect to the plasma that pulls electrons back into the source bottle and push ions to the accelerator column.

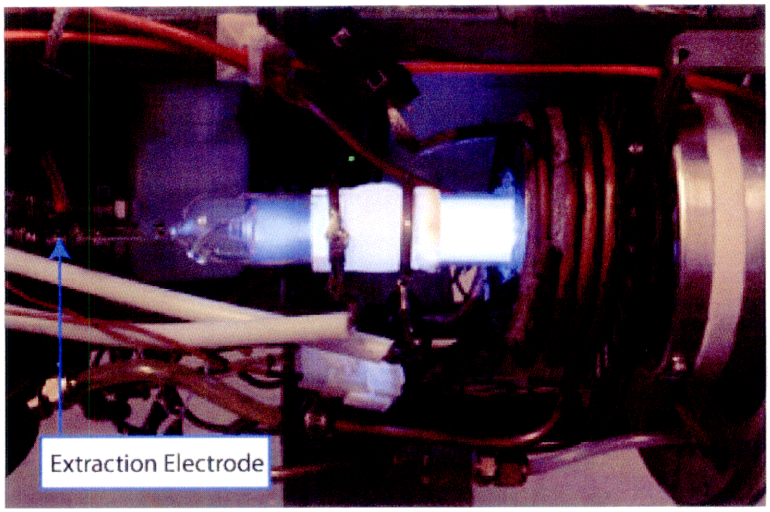

Figure 2- 3: ***Energized Ion Source.*** *The D_2 gas is accelerated through a variable leak valve. The gas is subsequently ionized by radiofrequency waves emitted by two RF rings positioned around the ion source bottle. The ion source is sitting on a potential of about 5kV, that allows the D^+ ions to be extracted into the accelerator column. The solenoid, shown to the right in the picture, compresses the particle beam when it is extracted into the accelerator column, and draws heat from the plasma. As a result, the solenoid-copper tubing is water cooled.*

Within the accelerator tube, a series of resistors gradually biases the system up to a maximum voltage of approximately 150 kV. Both the accelerating voltage and the extraction voltage can be controlled by the operator.

The target, which consists of either an erbium (Er) or titanium (Ti) disk fastened onto a copper end cap that is brazed to a water-cooled feedthrough, can be fully inserted into, or removed from, the beamline (and is shown in Figure 2- 4). These target materials are chosen because of their large affinities for hydrogen. Typically, a 120 kv, ~100 μA $^3He^+$ or D^+ beam is used to dope the targets. After 10 minutes, progressively lower potential/current beams are used for longer periods for a total doping time of ~1h.

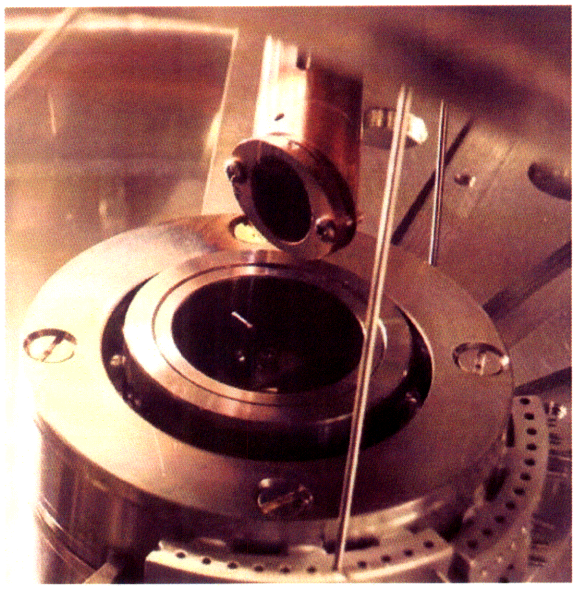

Figure 2- 4: ***Erbium Target.*** *The erbium target is positioned in the middle of the target chamber. The erbium disk is brazed onto a water-cooled feedthrough that can be inserted or removed from the beam line by a stepper motor mechanism. Erbium (or Titanium) is chosen because of their large affinities for hydrogen. Typically, a 120 kV, ~100μA $^3He^+$ or D^+ beam is used to dope the targets. After 10 minutes, progressively lower potential/current beams are used for longer periods for a total doping time of ~1h.*

2.2 Beam Profiler

As shown in Figure 2- 1 and Figure 2- 5, a beam profiler examines the beam before it enters the target chamber. The system, which consists of a wire that is swept through the beam path, is connected to a Tektronix TDS 3024B oscilloscope to allow for real time measurements of size, shape, position, and intensity of the beam. Beam spot sizes on target are typically between 5 and 12 mm in diameter depending on acceleration, extraction, and focus voltages. The profiler can either be used for positively or negatively charged particles. In addition, the beam profiler motor is always in operation and provides continuous data on the beam's profile (National Electrostatics 1.1).

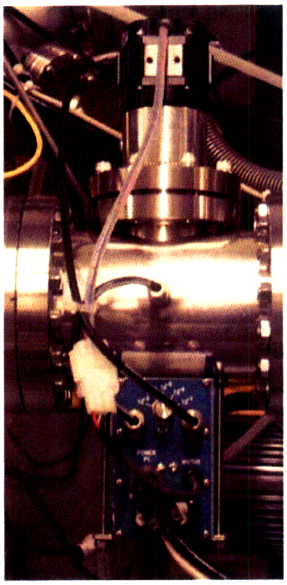

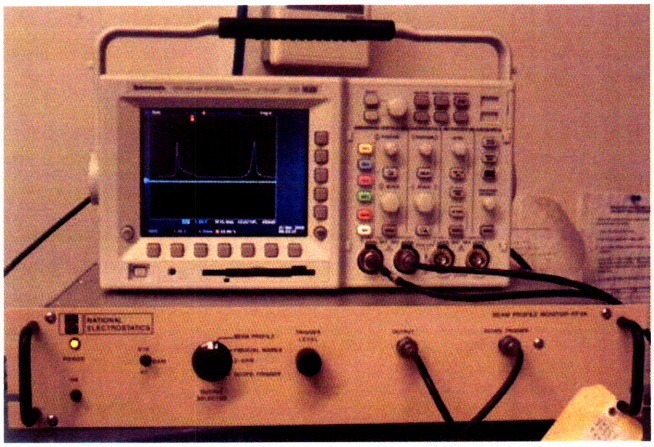

a *b*

Figure 2- 5: ***Beam Profile Motor, Oscilloscope, and Beam Profile Monitor.***
(a) The beam profiler system, which consists of a wire that sweeps through the beam path, allows for real time measurements of the size, shape, position, and intensity of the beam.
(b) Tektronix TDS 3024B oscilloscope, which displays the intensity and shape of the beam in two directions. The beam profile monitor is underneath the oscilloscope and receives signals from the beam profiler.

2.3 Fusion-product Generation and Reaction Rates

2.3.1 Fusion-product generation

By accelerating either D^+ or $^3He^+$ ions onto a ^3He or D-implanted Er or Ti target, either D-D reactions (reactions 2 and 3) or D^3He reactions will take place in the target. The latter reaction is expressed as:

$$D + {}^3He \rightarrow p\ (14.7\ MeV) + \alpha\ \ (3.6\ MeV) \qquad (9)$$

Reactions 3 and 9 produce 3 MeV and 14.7 MeV protons, respectively, which are primarily used to calibrate CR-39 samples.

In the accelerator, a silicon barrier detector (SBD) is used to detect the yield and energies of these fusion products. Prior to these experiments, this SBD detector and associated data acquisition system is calibrated using an alpha-emitting Radium (Ra-226) source.

2.3.2 Fusion Reaction Rates

The fusion reaction rate in the target can be expressed as (Atzeni 4):

$$R_{it} = n_i n_t \langle \sigma v \rangle_{it} \tag{10}$$

Where n_i and n_j represent the ion-number density in the beam and target, respectively, and $<\sigma v>_{it}$ is the reactivity (the reactivities for the D-D, D-T, and D^3He reactions is shown in Figure 2- 6 n_i is equal to the beam current divided by the product of charge per ion (e), beam particle velocity (v), and beam cross sectional area (A), and thus can be expressed as:

$$n_i = \frac{I_i}{e \cdot v_i \cdot A} \tag{11}$$

While n_t is equal to the number of stopped ions in the target (N_t) divided by the doped target volume (V):

$$n = \frac{N_t}{V} \tag{12}$$

By incorporating equations 11 and 12, equation 10 gives:

$$R_{it} = \frac{I_i}{e \cdot v_i \cdot A} \frac{N_t}{V} \langle \sigma v \rangle_{it} \tag{13}$$

Integrating expression 13 over time and doped target volume provides an expression of the total fusion yield for a specific reaction, i.e.:

$$Y_{it} = \frac{I_i N_t}{e \cdot v_i \cdot A} \langle \sigma v \rangle_{it} \Delta t \tag{14}$$

As shown by equation 14, the total fusion yield depends linearly on the absolute beam current. A measurement of the beam current is therefore important for optimally running an experiment. A Faraday Cup is used for this purpose as discussed in detail in Chapters 3 and 4.

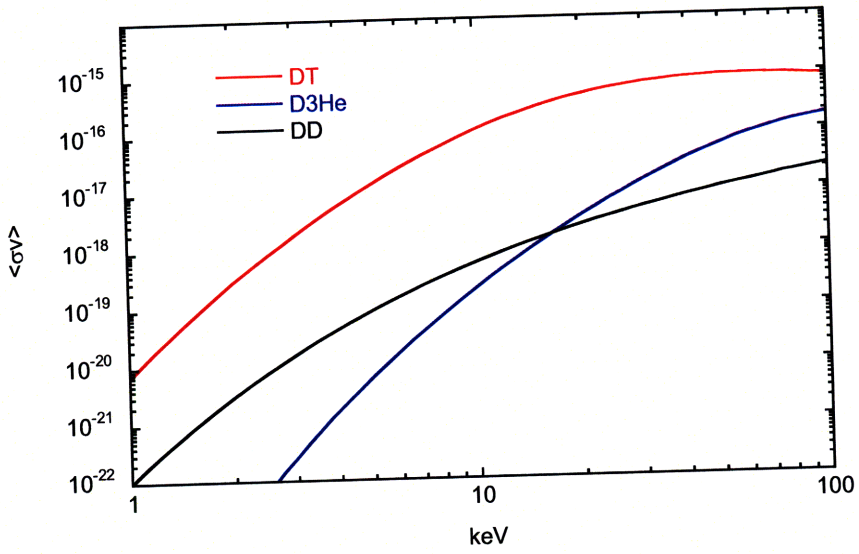

Figure 2- 6: ***Thermal reactivity as a function of ion temperature for fusion reactions of interest.*** The reactivity is shown for D-T, D-^{3}He, and D-D reactions at various energies. The accelerator runs D-^{3}He, and D-D reaction, but no tritium reactions.

3. Faraday Cup

3.1 Faraday Cup Physics Principles

A Faraday Cup is a conductive metal cup that captures charged particles. When particles hit the cup, a current (I) is generated that can be measured by an ammeter, which is linearly proportional to the number of ions striking the cup. The cup exhibits a certain level of flexibility as it can be biased to attract particles of specific charge. In these experiments, however, the beam is composed of only positively charged ions so the cup does not need biasing; it is simply left grounded.

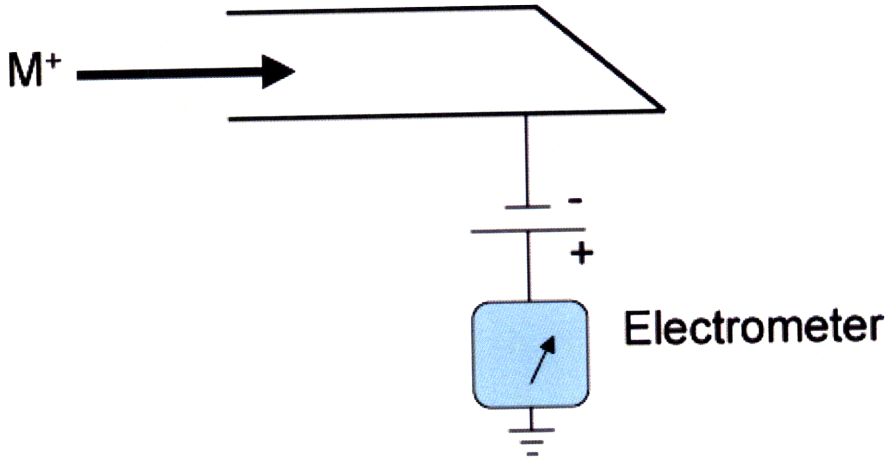

Figure 3- 1: ***A Schematic Electrical Diagram of the Faraday Cup.*** *When positively charged ions strike the Faraday Cup's metal surface a secondary current, proportional to the number of ions striking the cup, is generated that can be measured by an ammeter.*

From equation 11 the beam current striking the target can be expressed as:

$$I_i = n_i e \cdot v_i \cdot A \tag{15}$$

As the velocity of the beam ions can easily be expressed as the product of the charge and voltage. The beam current expressed in equation 15 can be rewritten as:

$$I_i = n_i e \cdot A \cdot \sqrt{\frac{2ZV}{m}} \tag{16}$$

where Z is the charge of the beam ion and V is the voltage potential.

3.2 Faraday Cup Hardware Specs

There are three BNC cables that connect to the Faraday Cup. One cable is for the high voltage to the secondary electron suppressor, which should be negatively biased between 500 and 800

volts to effectively suppress the secondary electron and to avoid arcing. The purpose of biasing the Faraday Cup is to prevent secondary electrons from leaving the surface of the cup. As the beam energy increases, the production and ejection of secondary electrons increases, which effectively increases the positive current measured by the ammeter. If the secondary electron suppressor is not applied to the Faraday Cup, a significant fraction of the secondary electrons escape resulting in an increased net current read by the ammeter. In addition, as the energy of the beam ions increases, there is a greater risk of a larger amount of secondary-electron ejection. To avoid this issue, the Faraday Cup is biased as high as possible as long as it will not cause any arcing.

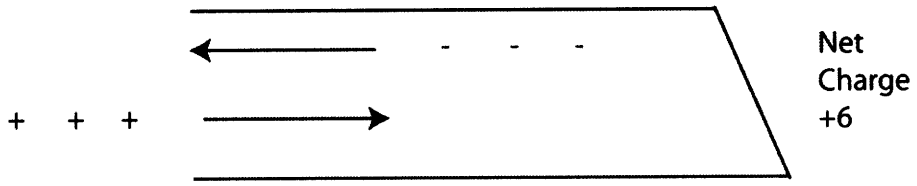

Figure 3- 2: ***A Schematic Drawing of the Faraday Cup when the Electron Suppressor Is Not Applied.*** *When positive beam ions, strike the Faraday Cup, secondary electrons are produced. If the suppressor is not in use, electrons are allowed to escape resulting in an increased net current.*

The second cable from the Faraday Cup connects to a Signametrics SMX 2060 Digital Multimeter (DMM) that reads the beam current. This ammeter has sensitivity down to sub-microamps. During a beam current measurement, the target is moved out of the beam to give a clean path to the Faraday Cup, which is positioned behind the target (see Figure 2- 1). After the current measurement has occurred, the target is moved back into the beam path for doping or for the main fusion experiment. A third BNC connecter (Blende) exists on the Faraday Cup, but this connector is not in use for this particular experiment. The Faraday Cup, which is manufactured by Princeton Scientific, does not require external cooling and is rated to handle beams up to ~600W.

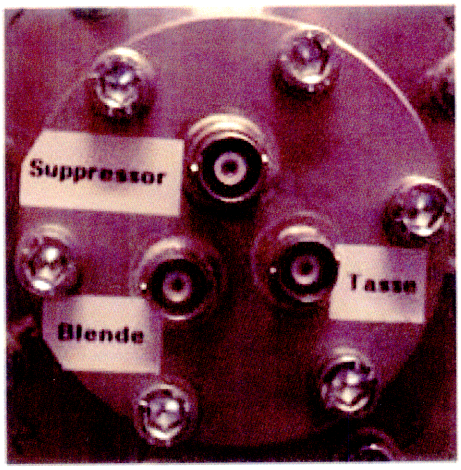

Figure 3- 3: ***The Backend of the Faraday Cup.*** *Three connectors exist on the back of the Faraday Cup as displayed. The "Suppressor" connector is a high voltage connector for the secondary electron suppressor, the "Tasse" connector is for the Cup's beam current measurement, and the "Blende" connector is not in use for the current Cup setup.*

3.3 Control Software

The Faraday Cup is operated using LabView that interacts with the Signametrics DMM to obtain the beam-current measurements. The procedures for operating the software and Faraday Cup are given in Appendix A. The current measured is simultaneously displayed in real time on the LabView front panel (GUI) and recorded in a data file to be reviewed and analyzed by the accelerator user. The software is currently configured to sample an averaged Faraday Cup once a second. Figure 3- 4 displays the input connectors for the DMM PXI cards, which can be configured to measure either current or voltage.

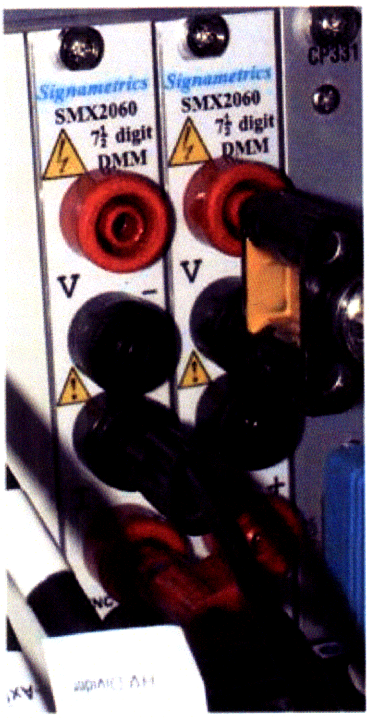

Figure 3- 4: ***Signametrics Card Inputs.*** *The DMM card on the left has connectors in the current terminals for measuring the beam current. The DMM card on the right has connectors in the voltage terminals for measuring the beam voltage. Both cards are installed on the PXI computer.*

4. Data

4.1 Calibration of the DMM PXI Card

The DMM card was calibrated by its manufacturer, but an additional test was performed using a 1-V voltage source and a 10 kΩ resistor to give a target amperage of 100μA.

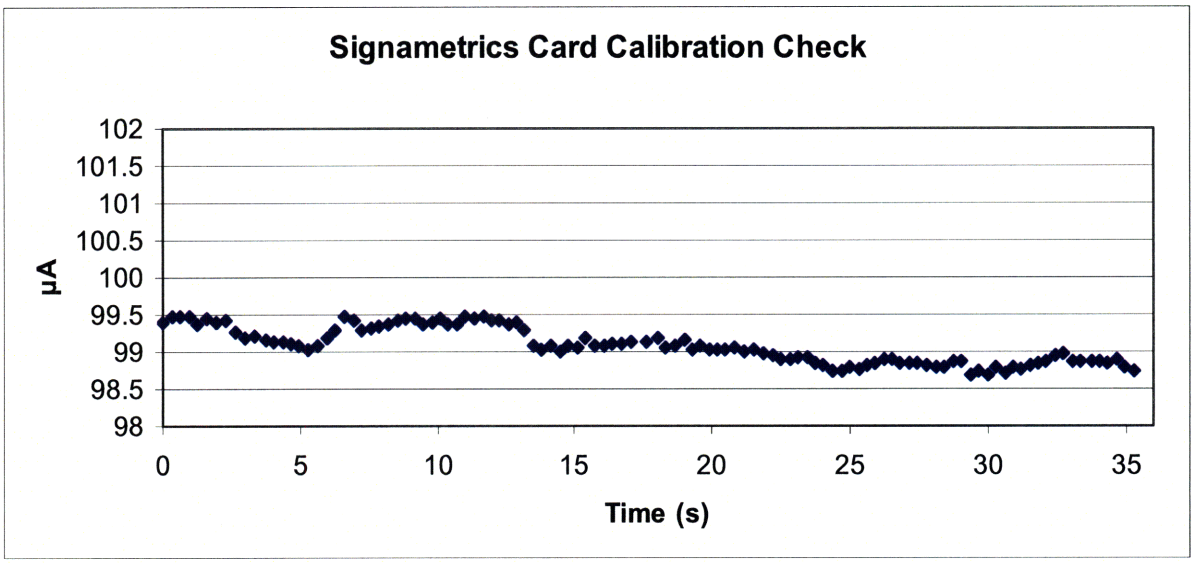

Figure 4- 1: ***Signametrics DMM Card Calibration.*** *The DMM was calibrated with a known voltage source to ensure accurate current measurements. Using a 1 V source with a 10 kΩ resistor, a current of ~100μA was generated. A slightly lower current was measured by the DMM card, and over time it drifted with ~0.5 μA. This is, however, consistent with the specified uncertainty of 0.5%.*

The readings from the DMM card are in microamps, and the measurements are consistent with the specified 0.5% error which confirms that the DMM card was in proper working order and would be able to correctly sample a current.

4.2 Beam-Current Dependency on Beam Voltage

When running the accelerator, the beam current changes depending on various conditions. Parameters that have an effect on the current are: voltage as described by equation 16, vacuum and the extraction voltage at the ion source.

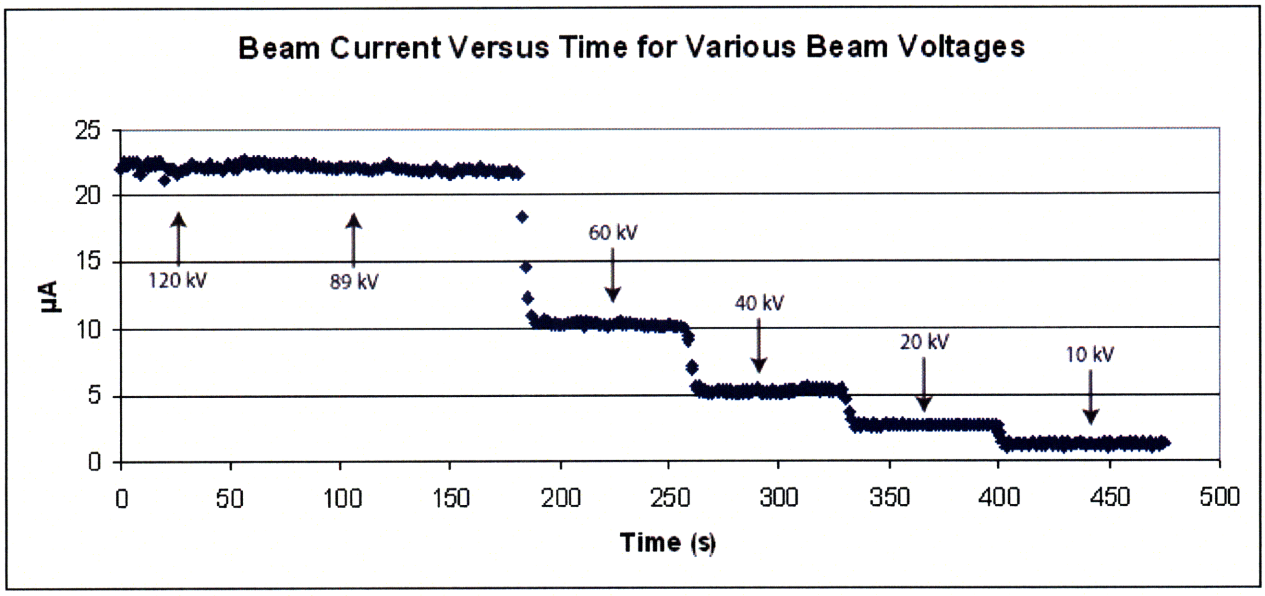

Figure 4- 2: ***Beam Current versus Time for Various Beam Voltages.*** *The extraction voltage was set at 3.2 kV, which is the optimum voltage for a 120 kV beam. The y-axis displays the beam current in microamps, which the x-axis displays time in seconds. As the beam voltage is changed the beam current is changed as well. At 120 keV, the beam is for this particular run is ~22 microamps, while at 10 kV it's ~1µA.*

The graph in Figure 4- 2 was taken by fixing the ion-source-extraction voltage while the beam voltage was initially set at 120 kV. The beam voltage was then reduced in steps as shown in Figure 4-2 and Table 4-1.

Time (Sec)	Beam V (kV)	Avg. I (mA)
0	120	0.02222
50	89	0.02208
145	60	0.01026
208	40	0.00526
267	20	0.00265
326	10	0.00128

Table 4- 1: ***Beam Voltage Over Time with Average Current.*** *Beam current is shown as a function of beam voltage.*

Combining equations 13 and 14 with the data from the Faraday Cup, the fusion rate can be determined, and the result of the current measurements is used to calculate theoretical rates from a 120 kV D^+ beam varying from 0 µA up to about ~140 µA results in fusion reaction rates shown in Figure 4-3.

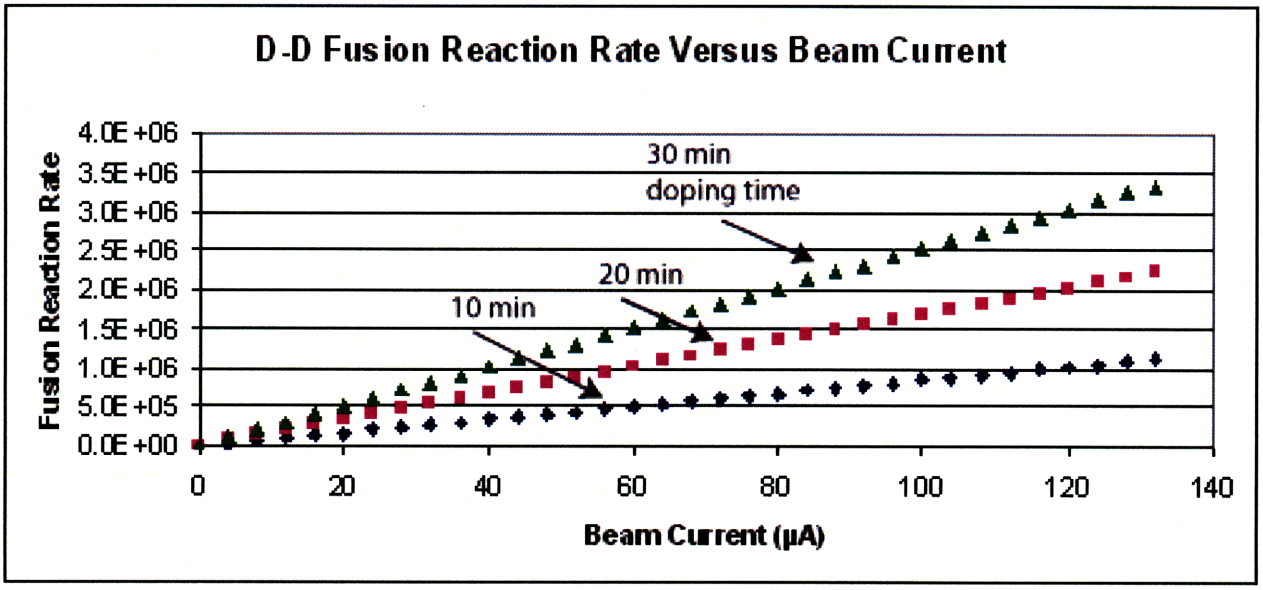

Figure 4- 3: ***D-D Fusion Rate Versus Beam Current.*** *The fusion reaction rate from section 3 was used to compute fusion rates in the accelerator using the beam current values from Table 4- 1. The plot assumes a fusion beam voltage of 120kV and a doping voltage of 40kV. The three plots are for different doping times of 10, 20, and 30 minutes.*

4.3 Suppressor On and Off

As discussed in Section 3.2, the suppressor voltage bias on the Faraday Cup prevents secondary electrons from leaving the surface of the cup and thus affecting the current measurement. A test was performed to see what an effect the suppressor had on the current. The average amperage of the test with the suppressor on was 21 μA. The reading was stable and the test was short to ensure that thermal expansion wouldn't affect the pressure and beam current during the run. The average amperage of the test with the suppressor off was 30 μA. Though this is almost a 50% increase in the current, more tests must be completed to determine whether there is an absolute or relative current change from turning the suppressor off. The tests were repeatable and do show that the suppressor affects the current measurement.

4.4 Vacuum Pressure Effects

The Faraday Cup data indicate a discrepancy in the beam currents at different vacuum pressures. For instance, in the beginning of a particular accelerator run when the vacuum pressure was

about 2.5×10^{-5} torr the beam current was 57 μA. After a period of 20-30 minutes, the temperature increase in the solenoid around the ion-source bottle caused the bottle to thermally expand to the point where the vacuum started to deteriorate, and in this particular case the vacuum pressure changed from 2.5×10^{-5} torr up to 8.2×10^{-5} torr. As the pressure went up, the beam current was significantly reduced from 57 μA to 42 μA. During these two tests, the beam profiles were also taken to compare how the profile relates to current changes (see Figure 4- 4). As indicated by the figure, the beam profile changed considerably, and the change seems to be qualitatively consistent with the Faraday Cup measurements.

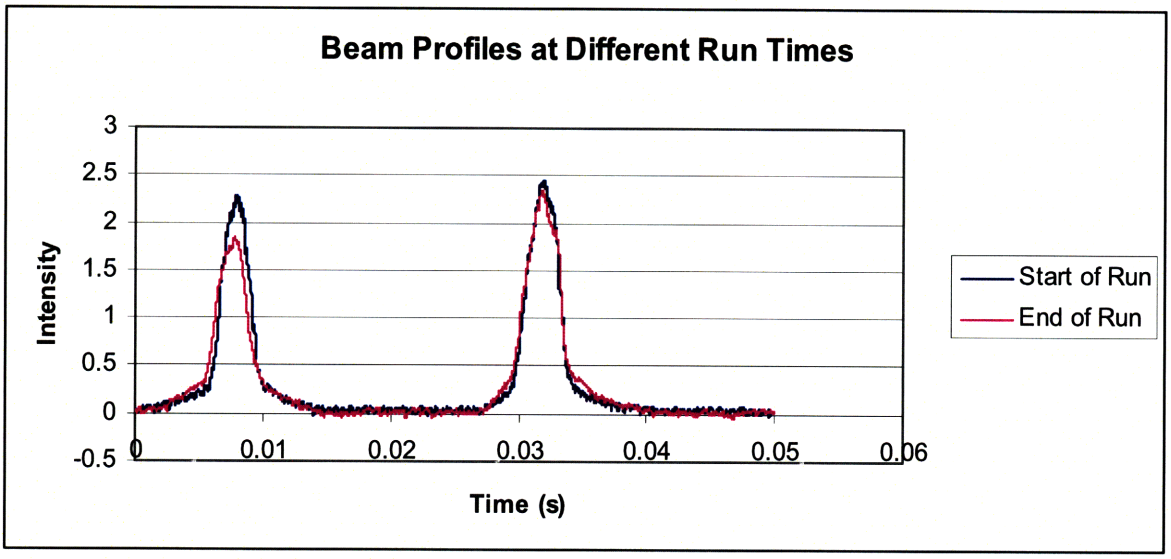

Figure 4- 4: ***Beam Profiles at the Start and the End of the Accelerator Run***. *The beam is of higher quality in the beginning of the run because the vacuum is stable. During the run the vacuum deteriorated, resulting in a broader beam with lower intensity, which seems to be in an agreement with the Faraday Cup measurement. Initially the beam current was 57 μA and at the end it was 42 μA.*

5. Conclusion

The Faraday Cup is a successful diagnostic for use in instrument calibration with the linear accelerator. Other experiments rely on proper prediction of reaction rates by the Faraday Cup.

For 100μA 120kV D^+ current on an erbium target doped with deuterium, D-D reaction rates of ~107 per second were determined. Besides the Faraday Cup, a target movement stepper motor was also successfully installed and tested, their LabView based control programs were written, and their operation procedures were documented. The secondary electron suppression capability of the cup was successfully tested as well.

6. Future Research Activities

There are other instrumentation adaptations for the particle accelerator that could help with these detector tests and calibrations. One possible example is the installation of an infrared camera in one of the target chamber ports. This device would provide visual confirmation of the beam striking the target.

While performing the Faraday Cup experiments, the beam current was affected by the pressure changes within the accelerator. This has been a recurring problem caused by the thermal expansion of the ion source bottle. For example, after a 20-30 minute run, the vacuum had deteriorated significantly resulting in lower beam current. Although ideally the thermal expansion problem should be solved by using a new glass metal connection for the bottle, there are pressure relationships with the beam current that could be explored before the replacement operation is complete. Even after completion, beam current dependence on pressure can be pursued.

Though the fusion reaction rates were calculated using a beam current, the confirmation tests for fusion product detection using the SBD were not completed. A number of accelerator failures and inconsistencies contributed to multiple temporary suspensions of accelerator use. The calculated fusion rates should be compared with the results of future CR-39 calibration tests and the detections registered by the SBD.

The thermal limitations of the Faraday Cup could be explored. The Cup is rated for 600W beams, but there was never any testing done in lab to ensure that the time duration of beam interaction could not potentially damage the cup.

Experiments can be performed to focus on the levels of Faraday Cup secondary electron suppression based on suppressor voltage bias. Before performing these tests, other variables such as

the operational accelerator pressure should be better controlled. These experiments could lead to a more ideal suppressor voltage setting for accurately finding the beam current.

The error associated with beam current measurements on the Faraday Cup has not yet been entirely quantified. Ideally, a predictable beam current based on beam voltage, extraction voltage, and pressure would be possible, though the individual contributions from each variable would have to be quantified.

References

Atzeni, Stefano and Jurgen Meyer-Ter-Vhen. The Physics of Inertial Fusion. Oxford: Clarendon Press, 2004.

Ballabio, L., et al. "α Particle Knock-on Signature in the Neutron Emission of DT plasmas". Physical Review E. Volume 55, Number 3. March 1997.

Casey, Dan, et al. "GEANT4 and TART modeling of the Magnetic Recoil Spectrometer (MRS) for absolute neutron measurements at OMEGA". Presented at American Physical Society, Dallas, Nov. 17, 2008

Frenje, Johan et al, "First measurements of the absolute neutron spectrum using the Magnetic Recoil Spectrometer (MRS) at OMEGA (invited)." Accepted for Publication in Rev. Sci. Instrum. (2008).

Huba, J.D. NRL Plasma Formulary. Washington D.C.: Naval Research Laboratory, 2007.

LLE Website. 2008. MIT. Accessed 15 Nov 2008. <http://www.lle.rochester.edu/>.

Lindl, J., et al. Physics of Plasmas. Vol. 2, No. 11, p. 3933. 1995. Accessed 9 Dec 2008. <http://fti.neep.wisc.edu/neep602/LEC26/IMAGES/fig29.GIF>

McDuffee, S.C., et al. "An accelerator based fusion-product source for development of inertial confinement fusion nuclear diagnostics," Rev. Sci. Instrum. 79 (2008) 043302.

McRory, R. L., et al. "Progress in Direct-Drive Inertial Confinement Fusion". Physics of Plasmas. 15, 2008. <http://www.psfc.mit.edu/hedp/Home%20Page/Papers/McCroryPoP2008.pdf>

MIT PSFC Website. 2008. MIT. Accessed 15 Nov 2008. <http://www.psfc.mit.edu/research/hedp/>.

Murray, K. "Faraday Cup". 12 April 2007. Accessed 1 Nov 2008. <http://upload.wikimedia.org/wikipedia/commons/5/57/Faraday_Cup.png>

National Electrostatics Corporation. Instruction Manual for Operation and Service of Beam Profile Monitor Model BPM80. 1995.

NIF Website. 2008. LLNL. Accessed 15 Nov 2008. <https://lasers.llnl.gov/>.

National Instruments. "User Guide MID-7604/7602 Power Drive". January 2006. Accessed 20 Sept 2008. <http://www.ni.com/pdf/manuals/372454e.pdf>.

Seguin, F.H. et al., "Spectrometry of charged particles from inertial-confinement-fusion plasmas", Rev. Sci. Instrum 74 (2003) 975.

Appendix A: Faraday Cup Operation

A.1 Faraday Cup Initiation and Operation

The Faraday Cup allows for measurements of the beam current in the accelerator. The current measured is proportional to the number of ions in the beam. This guide explains and shows the daily operation procedure for the Faraday Cup.

1. Before the accelerator is turned on, the suppressor voltage for the Cup must be turned on. Channel 1 of the voltage supply is currently connected to the suppressor, which will keep secondary electrons from escaping the surface of the cup. The voltage is negatively biased and set to 550V, and should not be increased above 800V. The switch must be moved from Disable to Enable.

Figure A- 1: ***Suppressor high voltage supply switch.*** *The switch must be moved from "Disable" to "1 kV" in order to activate the secondary electron suppression mechanism of the Faraday Cup. The range dial adjusts the voltage bias on the suppressor, but in order to see the voltage on the digital readout, the upper knob must be turned to the appropriate channel.*

2. To take an accurate beam count, the target must be moved out of the beam's path. The target stepper motor can be used to move the target. Appendix B describes information on the target stepper motor and its operation.
3. The LabView software must be initialized. The current readings will be obtained when the program begins to run. When the user is done obtaining readings, he or she can stop the program. The measurements will be recorded in a data file in the directory of the VI.
4. After measurements are finished, the target must be reinserted for experiments, again using the target stepper motor.

5. After returning the target to the beam line-of-sight, the accelerator can be run normally for doping and reaction runs.

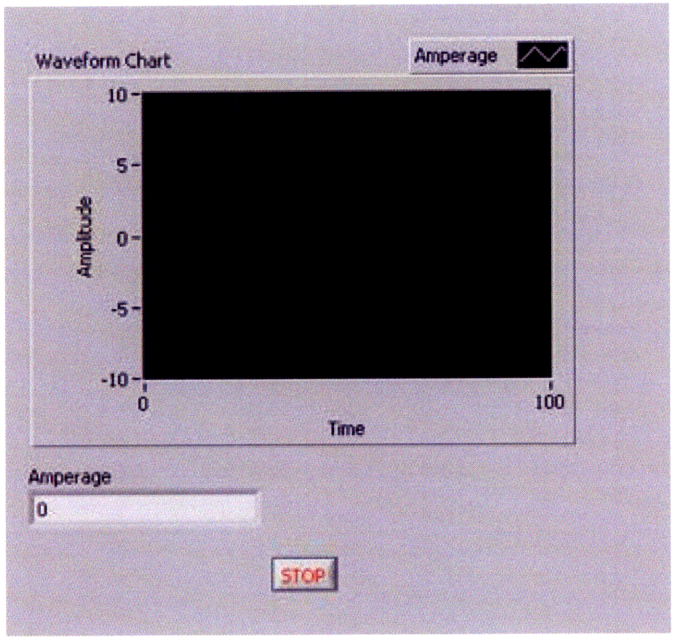

Figure A- 2: ***VI front panel for the Faraday Cup.*** *The VI front panel outputs both a graph of the beam current measurement over time (and retaining data from previous measurements), as well as the real time most recent measurement. The data is recorded in a data file for recall and analysis. All current values are given in milliamps. The "STOP" button ends the measurement program's operation.*

The front panel of the Faraday Cup measurement VI has an indicator that shows each current measurement. There is also a graph that shows the time evolution of the current readings. Figure A- shows the Faraday Cup front panel. The measurements are given in milliamps.

A.2 Cup Shutdown

After shutdown of the accelerator:

1. The Faraday Cup VI must be shutdown.
2. The suppressor voltage must be disabled.

A.3 Cup VI

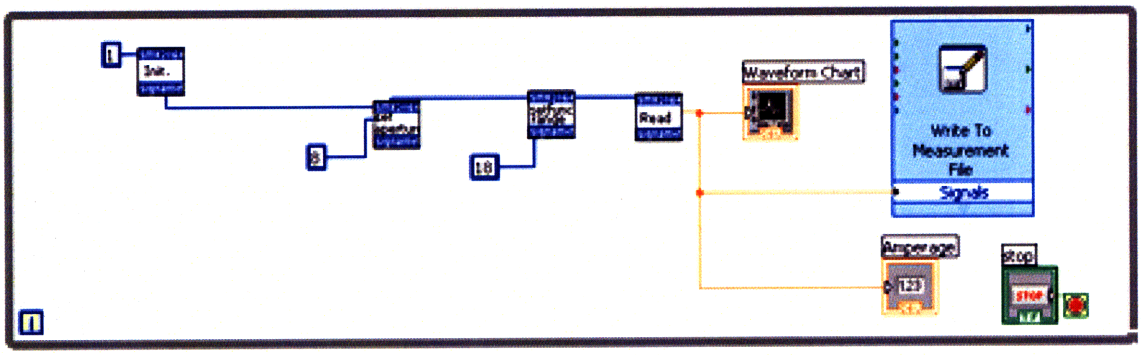

Figure A- 3: ***Faraday Cup VI block diagram.*** *The code of LabView is displayed, including the blue boxes on the left, which customize configuration settings for the DMM such as aperture sampling rate, range of measurement, and type of measurement. These parameters must all be defined so that default values are not inadvertently used. The orange box outputs the data to the graph and indicator, while the blue box in the upper right writes the measurements to a file.*

The block diagram for the Faraday Cup VI is given in Figure A- 3. The file names can be controlled in the "Write to Measurement File" Express VI block. The sampling aperture time can be determined in the relevant block. Other programs utilizing DMMs must be sure to define all parameters, because default conditions are overridden if other programs are using those functions. There was initially a problem with the Accelerator Controls VI that needed an extra code block to fix an error when simultaneously running with the Faraday Cup program. There is no longer an issue, but it will be important for future program design.

Appendix B: Stepper Motor Installation and Operation

B.1 Stepper Motor Overview

For an accurate measurement of the beam current, the Faraday Cup must have a clean line-of-sight of the beam, so frequent movements of the target in and out of the beam path are necessary. A stepper motor driven target mechanism has the advantage of not requiring human eye alignment, and can be positioned precisely each time it is in use. The system allows the operator more specificity over the target movement from the control room. Limit switches are positioned so that the motor will not over-insert or remove the target, causing damage to the accelerator or target chamber.

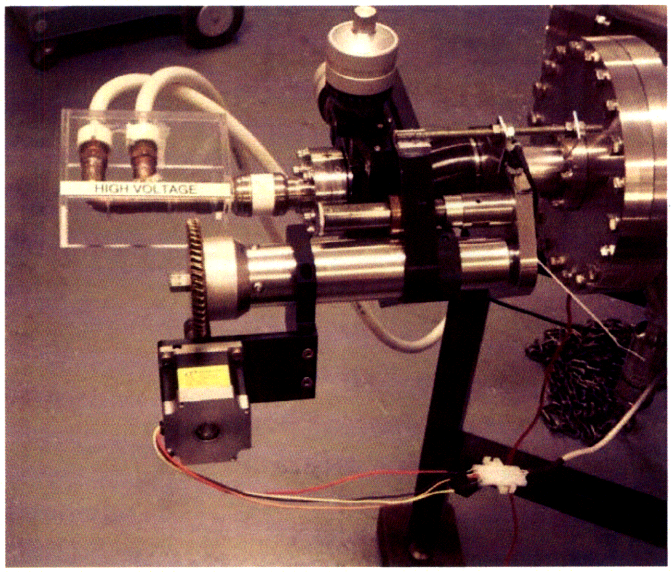

Figure B- 1: ***Motor Setup.*** *The stepper motor is positioned in the lower left of the picture and is connected to an NI power drive. The motors drives the mechanism that can insert or remove the accelerator target into or from the target chamber.*

The CT series stepper motor from Danaher Motion was chosen to make use of the limited current available from the power drive. The motor currently in use, a Danaher Motion motor of model number CTM21NLF15NAAOO, has a maximum current load of 1.5 amps. The power drive can deliver up to 1.4 amps, and the Danaher engineers recommended the 1.5 amp model. A 1.0 amp motor is also available for use, though the 1.5 amp model has faster performance, which is more ideal for its intended use as part of the target insertion mechanism.

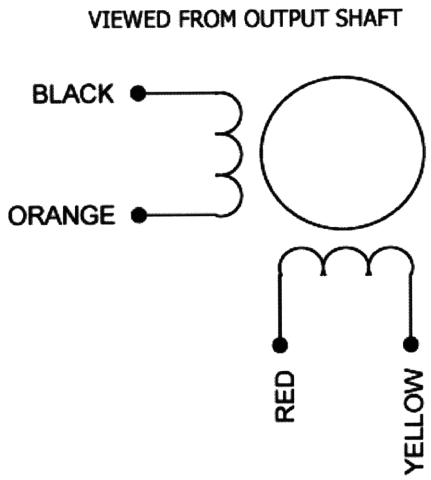

Figure B- 2: ***Stepper Motor Wiring Phases.*** *The diagram for the Danaher Motion 4-lead motor shows the colored wires and phase loops for connection to a power drive.*

Figure B- 2 shows the wiring diagram for the phases of the 4-lead stepper motor. Current must be delivered to the motor in a specific square wave pattern to activate the stepper motor magnets and drive the motor rotation.

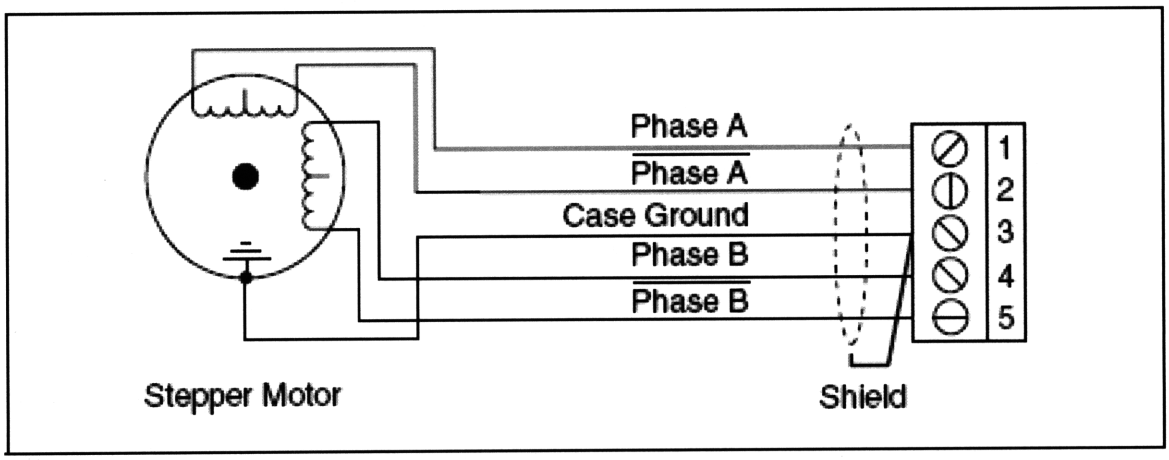

Figure B- 3: ***Phase Diagram for National Instruments Power Drive.*** *The phase loops for connection to a power drive are shown. In conjunction with Figure B- 2, these two diagrams show the specific method for connecting the motor and power drive.*

Figure B- 3 shows the circuit diagram for the NI power drive and the arrangement for a 4 lead stepper motor. In the current setup of the stepper motor, the yellow lead is connected to port 1, the red lead is connected to port 2, the orange lead is connected to port 4, and the black lead is connected to port 5. Port 3 remains unconnected, as it is optional extra grounding.

Switch	Peak Output (A)
	1.40

Figure B- 4: ***National Instruments Power Drive Current Settings.*** *The current setting on the power drive is used to determine the peak current that will be sent from the power drive to the stepper motor.*

Figure B- 4 shows the configuration on the power drive for the peak current output to the stepper motor. The maximum output is 1.40 amps, and should be used because the current capacity of the stepper motor is 1.5 amps. If a stepper motor with a lower capacity is used, this amperage should be reduced.

Switch	Microsteps/Step
	10 (factory default)

Figure B- 5: ***National Instruments Power Drive Microstep Settings.*** *The current setting on the power drive is used to determine the signal patterns sent from the power drive to the stepper motor.*

Figure B- 5 shows the settings on the NI power drive for microsteps per step. The factory default is 10 microsteps per step, which works for the motor. Deviations from this setting may potentially disrupt motor function. The other stepper motors in use on the accelerator also use this setting.

B.2 Limit Switches

In order to prevent excessive movement possibly damaging the motor or target chamber, two hard limit switches are installed. They each prevent either forward or backward motor movement and cease motor movement when they are switched.

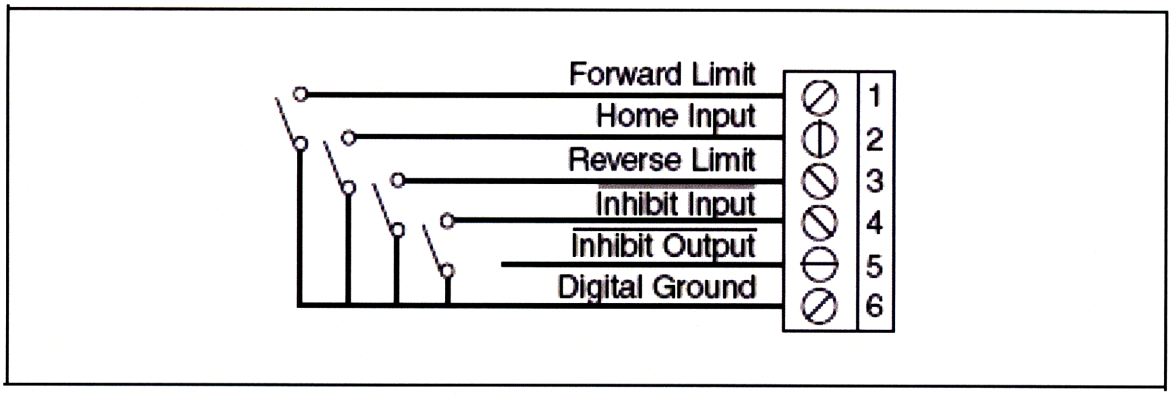

Figure B- 6: ***Limit Switch Pin Assignment on the NI Power Drive.*** *The limit switches allow physical boundaries to be established in the stepper motor's operation. When these boundaries are reached, signals are sent to the power drive, which then stops sending movement signals to the stepper motor.*

One limit switch is connected to the Forward Limit (pin 1), and the other limit switch is connected to the Reverse Limit (pin 3). They only prevent movement in their own specifically assigned direction.

B.3 Motor Operation

The motor is operated using a LabView Virtual Instrument (VI). The computer connects to the NI power drive, which operates the stepper motor. The VI controls motor movement and system calibration.

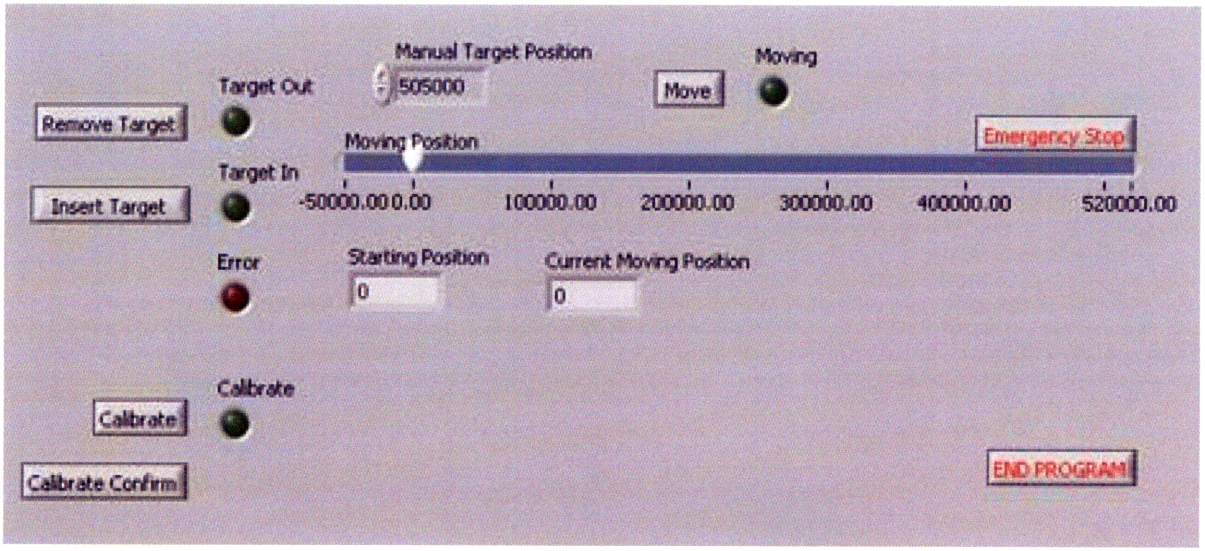

Figure B- 7: ***Main Front Panel of the Target Chamber Motor VI.*** *The front panel of the stepper motor program is used for all motor operations. The user has the ability to manually or automatically control the stepper motor.*

Figure B- 7 shows the main front panel of the motor movement program. To end the program,

there is an "END PROGRAM" button in the lower right. There is also an "Emergency Stop" button to halt motor movement during any motor operation.

B.4 Calibration

The stepper motor loses calibration when either the NI system is reset or the target is moved by hand. In the event that the target is not positioned correctly or a limit switch is inadvertently activated, the motor will have to be recalibrated. Recalibration will redefine the numbering system used by the VI to position the motor and will ensure that the "Insert Target" and "Remove Target" buttons assign the correct value.

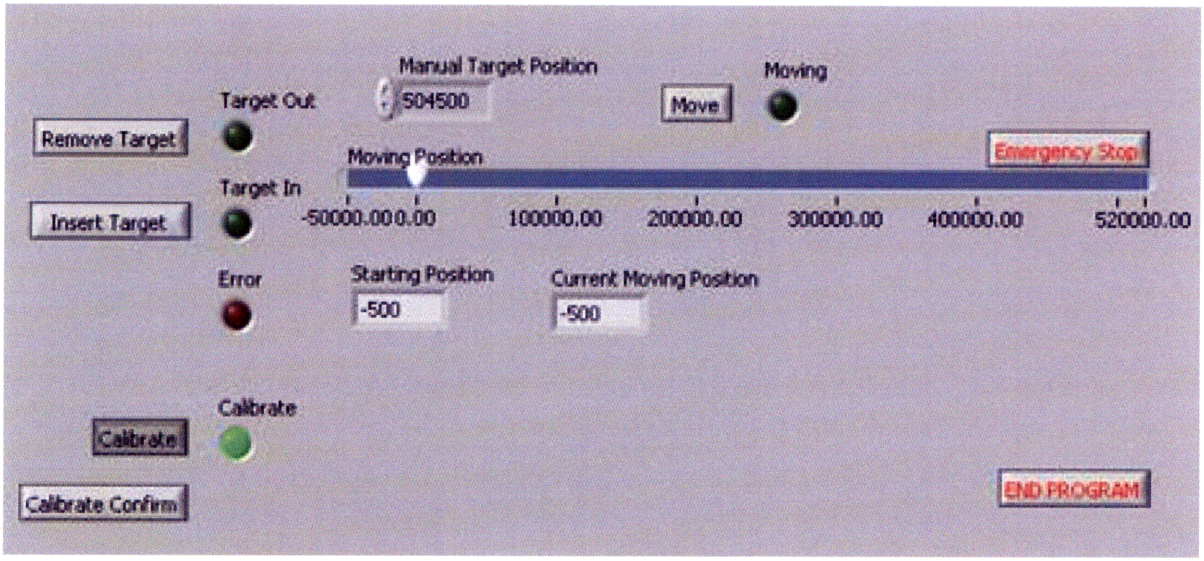

Figure B- 8: ***Main Panel while Calibrating.*** *During target calibration, the "Calibrate" button will be depressed as the motor is moving.*

Figure B- 8 shows the front panel during calibration. To calibrate, the user must click the "Calibrate" button, and then click the "Calibrate Confirm" button. The VI will then move the motor to the lower limit switch to establish a base number for the motor's position. It will then automatically add the distance necessary to reach specific target positions.

B.5 Target Insertion

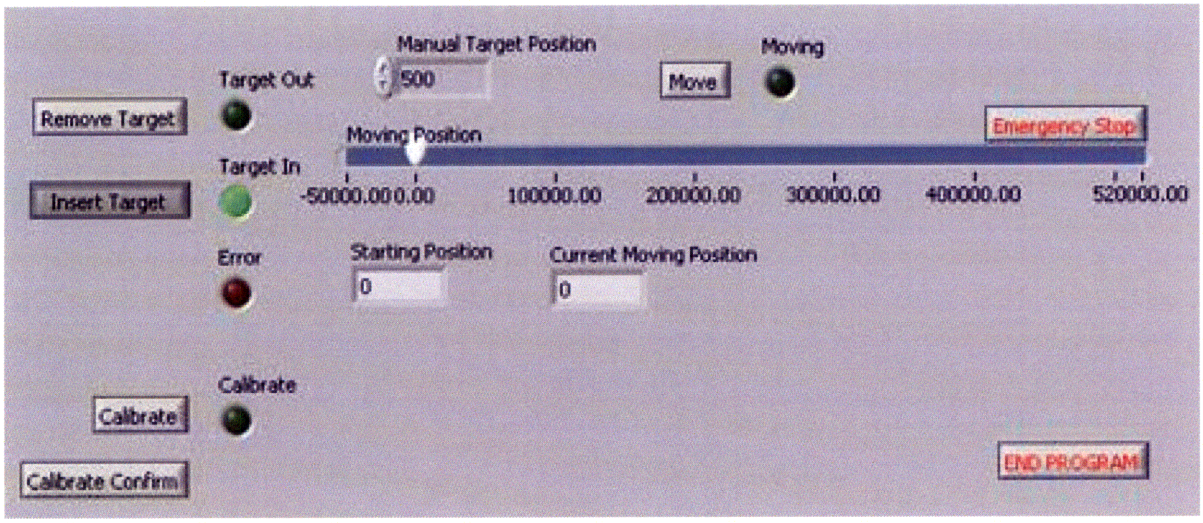

Figure B- 9: ***Main Panel During Target Insertion.*** *. During target insertion, the "Insert Target" button will be depressed as the motor is moving.*

Figure B- shows the main panel before target insertion. To insert the target, the user must push the "Insert Target" button. A green light will turn on to indicate the planned position of the target. After the green light turns on, clicking the "Move" button will confirm the movement selection and change the position of the target. The target can be tracked from the indicators that relay the position both graphically and numerically. The green "Move" light will be lit while the motor is moving to a specified position.

B.6 Target Removal

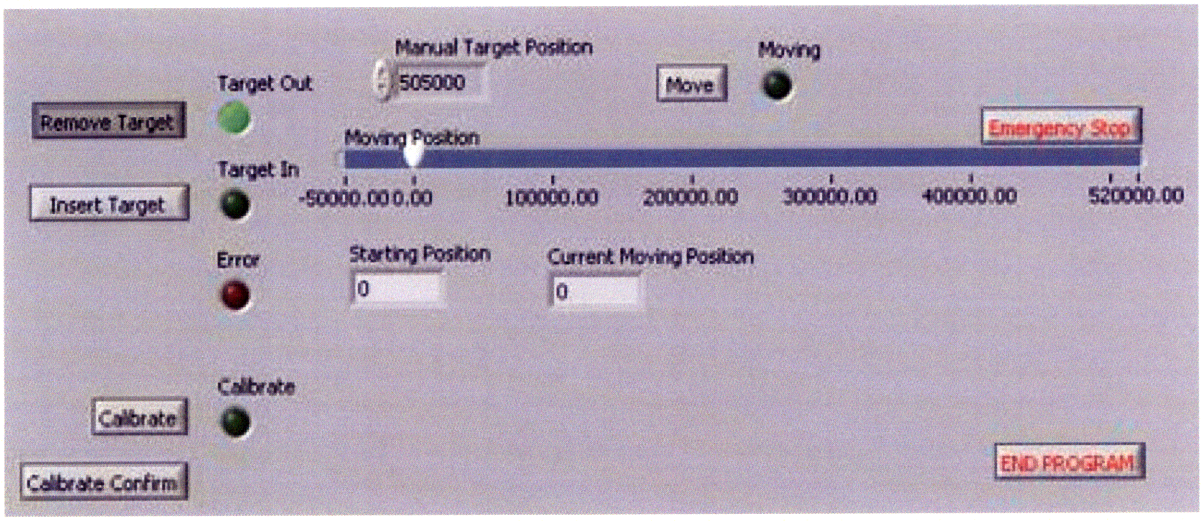

Figure B- 10: ***Main Panel during Target Removal.*** *During target removal, the "Remove Target" button will be depressed as the motor is moving.*

Figure B- 10 shows the main panel during target removal. This function works in the same manner as target insertion.

B.7 Motor Error

When both the "Insert Target" button and the "Remove Target" button are depressed at the same time, the red "Error" light will turn on, indicating that there is confusion about which action the VI should perform.

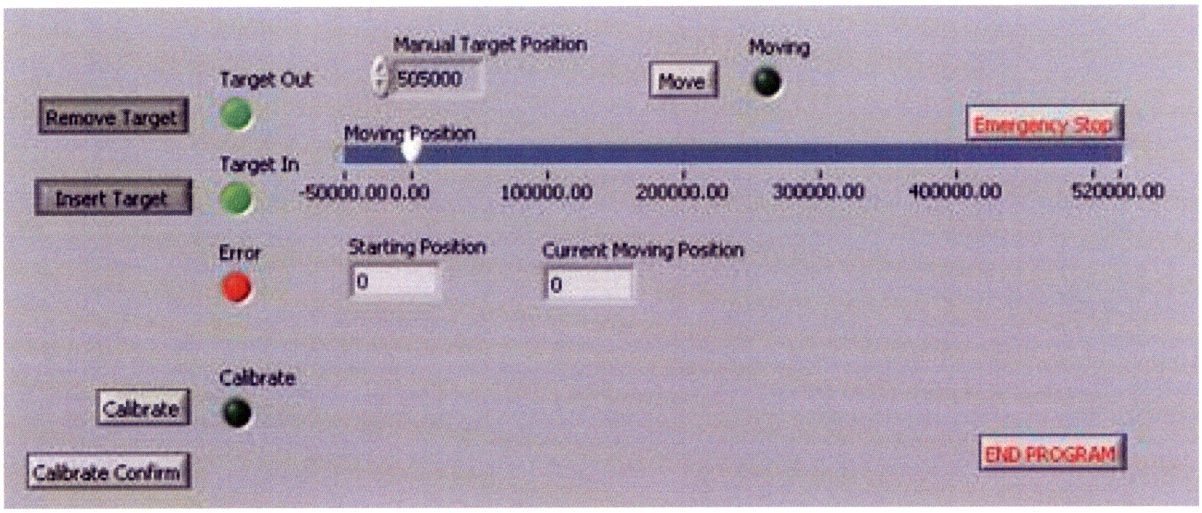

Figure B- 11: ***The Main Panel Displays an Error with Mixed Instructions.*** *The program has a built in warning light to show when conflicting instructions have been input.*

Figure B- 11 displays the error light when the two target location buttons are selected. To turn off the error, one of the two "Target" buttons must be unselected.

Manual Movement

The target can also be "manually" moved by inputting a number into the "Manual Target Position" control. This can be used for fine tuning the target position for a specific experiment.

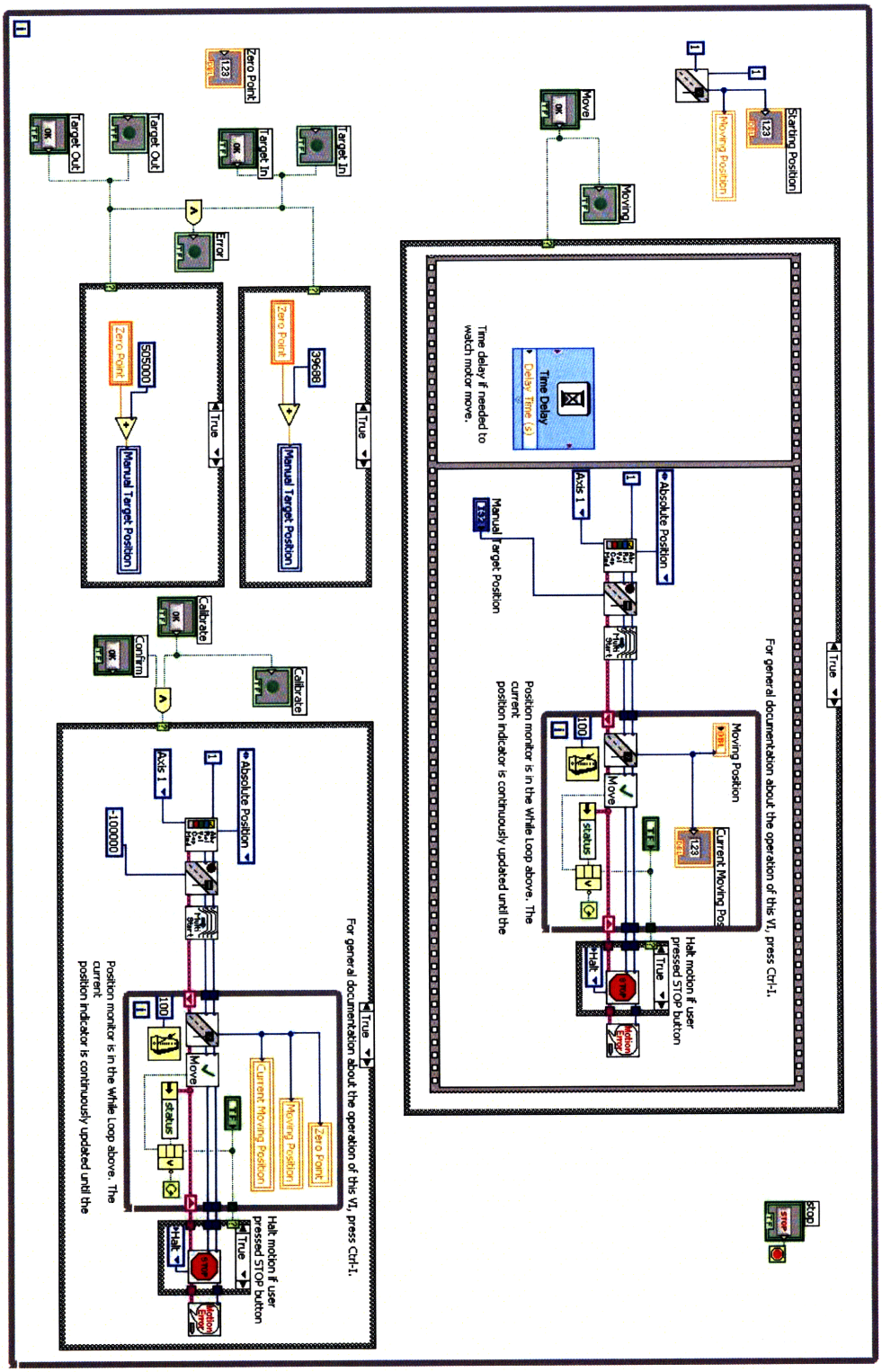

Figure B- 12: ***Stepper Motor Block Diagram.*** *The LabView code is displayed including loops for the calibration of the motor as well as its movement.*